Eurasia Journal of Science and Technology
Print ISSN: 2663-1024
Online ISSN: 2663-1016
DOI: https://doi.org/10.61784/ejst3169

POST-EARTHQUAKE SERVICE LOSS ASSESSMENT AND CRITICAL SEGMENT IDENTIFICATION IN GAS NETWORKS UNDER SPARSE MONITORING

Yu Cao[1], Tian Cheng[1,2], ChengCheng Jing[1], JiaoJiao Li[2,3*], WenKai Chen[1], SiQin Wang[1], YuTong Liu[1]
[1]*School of Energy and Power Engineering, Guangdong University of Petrochemical Technology, Maoming 525000, Guangdong, China.*
[2]*Guangdong Provincial Key Lab of Petrochemical Equipment Fault Diagnosis, Guangdong University of Petrochemical Technology, Maoming 525000, Guangdong, China.*
[3]*School of Chemistry, Guangdong University of Petrochemical Technology, Maoming 525000, Guangdong, China.*
[*]*Corresponding Author: JiaoJiao Li*

Abstract: During strong earthquakes, multiple pipeline segments in long-distance natural gas networks are often damaged within a similar timeframe. Whether damage to a pipeline segment results in service interruption depends on its location within the network and the availability of alternative routes; stations along the pipeline network are sparsely distributed, with individual segments spanning hundreds of kilometers, requiring the seismic field to be extrapolated based on both physical attenuation and field measurements. Taking the *Mw* 6.6 earthquake in central Italy on October 30, 2016, as an example, we assessed post-earthquake service consequences on a natural gas transmission pipeline network comprising 168 pipeline segments with a total length of 7,704.6 km: Using the physical attenuation from ITA18 as the far-field trend and residual Kriging from 175 stations as the near-field correction, 1,000 spatially correlated seismic motion scenarios constrained by observations were generated; Pipeline segment status was determined for each scenario based on publicly available vulnerability relationships, and network consequences were quantified using the service loss rate and gas supply connectivity rate; the service loss rate was then allocated to individual pipeline segments according to Shapley values, multiplied by the expected failure probability to obtain a risk-weighted score, which was used to establish inspection priority rankings. The results show that: in a scenario where gas enters only through two southern access points, the service loss rate for this pipeline network during this earthquake is 0.334, with an average of 12.1 pipeline segments failing; the service loss exhibits a bimodal distribution, with the number of failed segments differing by only 2.1 between the two peaks, yet the loss differing by a factor of 29—the difference lies in whether the failures occur on the sole route serving the northern demand nodes; Eighteen of the top 20 pipeline segments by risk-weighted score were located along this route, constituting the priority targets for post-earthquake inspections. If the three cross-border access points in the northern part of the pipeline network were also counted as gas supply entry points, the service loss rate dropped to 0.032, the bimodal distribution disappeared, and this route no longer constituted a bottleneck. This method can provide a reference for post-earthquake inspections and emergency decision-making in long-distance natural gas pipeline networks under conditions of sparse monitoring stations.
Keywords: Natural gas pipeline network; Conditional random simulation; Spatially correlated ground motion; Service loss; Shapley value

1 INTRODUCTION

Oil and gas pipeline networks may experience pipe segment failure and interruptions under seismic loads; therefore, post-earthquake assessments must not only determine the extent of damage to pipe segments but also analyze whether such damage causes gas supply interruptions and the scope of their impact [1-3]. This is because seismic wave propagation and permanent ground deformation can cause leaks or ruptures in buried pipelines, and whether these damages lead to widespread service interruptions depends on the connectivity between gas supply inlets, demand nodes, and damaged pipe segments. For example, during the 1995 Kobe Earthquake in Japan, damage to the pipeline network and emergency service suspensions left approximately 859,000 customers without gas, and it took 85 days to restore service [4]. For long-distance, cross-regional pipeline networks, seismic motion intensity varies spatially along the route; limited station records cannot directly cover all pipeline sections, and the consequences of simultaneous damage to multiple sections are jointly constrained by both the main trunk lines and alternative routes. Therefore, post-earthquake assessments must not only estimate seismic motion at locations without observation stations based on existing data but also translate localized damage into network service losses to determine which pipeline sections should be inspected first.
Regarding the assessment of seismic damage consequences in pipeline networks, existing research is gradually expanding from segment-level damage estimation to spatial hazard characterization and network functionality evaluation. At the pipeline segment level, empirical relationships established based on seismic damage records can utilize seismic motion indicators such as peak ground velocity (PGV) to estimate pipeline repair rates or failure probabilities. By describing differences in vulnerability among pipelines through attributes such as pipe material and joints, these models provide a foundation for regional pipeline network analysis [5-6]; Regional risk studies on natural gas transmission pipelines also

© By the Author(s) 2026, under the CC BY-NC-ND license (http://creativecommons.org/licenses/by-nc-nd/4.0).

indicate that uncertainties in vulnerability models and pipeline attribute information can affect damage and loss estimates [5]. Therefore, when generalizing single-point vulnerability relationships to widely distributed pipeline networks, it is necessary to characterize the joint distribution of seismic ground motion experienced by individual pipeline segments. Based on an analysis of strong-motion records from multiple events in Europe, PGV residuals exhibit spatial correlation that decays with the distance between stations; therefore, ground motion at different locations should not be treated as independent random inputs [7]. Building on this, the conditional multivariate normal method combines ground motion prediction models with observed records to infer intensity and its uncertainty at unobserved locations [8]; a study on the Italian earthquake further discussed the impact of site effect characterization and spatially correlated models on post-earthquake ground motion estimation [9]. Regional ground motion prediction models, meanwhile, provide empirical constraints on the effects of magnitude, distance, and site conditions on intensity and can serve as predictive trends for areas with insufficient observations [10]. These studies provide a basis for constructing hazard fields under sparse station conditions; however, in long-distance pipeline networks, it is still necessary to consider the relative distribution of pipeline segments and monitoring stations to clarify the regional scope within which station observations can effectively refine seismic motion predictions, verify the reasonableness of prediction results in areas far from monitoring stations, and analyze the impact of uncertainties in seismic motion estimates on the assessment of gas supply interruptions in the pipeline network. At the network scale, analyses of water supply service capacity considering spatially correlated ground motion and simulation-based evaluations of gas network connectivity have linked component damage to system functionality; simultaneously, gas network risk decomposition has been used to identify the contribution of components to system risk [1, 11]. This indicates that service loss cannot be explained solely by the number of failed pipeline segments but also depends on the substitution relationships between damaged locations and paths. To this end, the Shapley value in cooperative games—which measures the importance of network components by averaging marginal contributions across different combinations—provides a method for addressing the interactions among components [12-13]. However, contribution based on network structure does not directly account for the probability of pipeline segment damage during a specific earthquake, and simply ranking based on damage probability fails to reflect the consequences of gas supply disruptions. Both approaches have their own emphases and are difficult to apply directly to post-earthquake inspection prioritization. Therefore, for long-distance oil and gas pipeline networks with sparse monitoring stations, it is necessary to integrate spatially correlated seismic motion scenarios constrained by observations, network service losses, and pipeline segment structural contributions to establish a method for identifying critical pipeline segments that simultaneously reflects both event hazard and the role of gas supply pathways.

Building on the aforementioned research, this paper addresses the assessment of initial post-earthquake service consequences and the identification of critical pipeline segments in long-distance oil and gas pipeline networks under sparse station conditions. Using the October 30, 2016, Norcia earthquake in central Italy and a natural gas transmission network comprising 168 pipeline segments as a case study, we construct an analytical workflow consisting of seismic motion scenario generation, pipeline segment failure determination, service loss calculation, and inspection prioritization. First, the attenuation trend was derived using the ITA18 seismic motion prediction model. Kriging correction was applied using observation residuals from 175 monitoring stations to generate 1,000 sets of spatially correlated seismic motion scenarios constrained by observations. Through a “leave-one-out” test and segment-scale comparisons, the study analyzed prediction differences and far-field applicability resulting from various hazard field structuring methods; Subsequently, the status of pipeline segments is assessed through scenario-by-scenario sampling based on empirical vulnerability relationships. Gas supply connectivity and service loss rates are defined based on the connectivity between demand nodes and gas supply inlets, and the distribution of service losses and the impact of critical gas supply pathways on consequences are analyzed; Finally, Shapley values were calculated using pipeline segments as participants and the service loss caused by the removal of a set of segments as the objective function. By combining these values with the expected damage frequency, risk-weighted scores were derived to identify critical pipeline segments and compare the results with rankings based solely on structural contribution or damage probability. The above analysis links hazard estimation under sparse observation conditions with pipeline segment ranking based on network supply functionality, providing a basis for post-earthquake inspection and emergency resource allocation in long-distance oil and gas pipeline networks.

2 BASIC THEORY

2.1 Construction of Seismic Scenarios Using Regression Kriging

Under conditions of sparse observation stations, the seismic motion field must be extrapolated, and every single method has significant limitations. Pure interpolation methods offer high accuracy in areas with dense station networks, but their effective range is limited by the range of the variogram; predicted values for pipeline sections beyond this range collapse to a single constant. Pure physical attenuation models can provide trends of attenuation with distance in the far field but do not utilize actual station measurements, making it impossible to correct for local deviations in site effects and path effects. This paper employs regression Kriging [14-17]: physical attenuation is used as the conditional mean to capture the far-field trend, while spatial interpolation of station residuals is used to correct the near-field; spatially correlated random fluctuations are then generated around the conditional mean, thereby simultaneously satisfying the requirements for far-field behavior and near-field accuracy.

The hazard model selected is ITA18, which is suitable for shallow crustal earthquakes in Italy. RotD50 PGV is used as the intensity indicator, and the median value prediction formula is [10]

$$\ln \mathrm{PGV}_{\mathrm{med}} = \mathrm{FM} + \mathrm{FD} + \mathrm{FS} \tag{1}$$

In the equation, FM, FD, and FS represent the magnitude term, distance term, and site term, respectively. The specific expressions are

$$\mathrm{FM} = a + b_2(M_w - M_h), (M_w > M_h) \tag{2}$$

$$\mathrm{FD} = [c_1(M_w - M_{\mathrm{ref}}) + c_2]\log_{10} R + c_3 R \tag{3}$$

$$R = \sqrt{R_{jb}^2 + h^2} \tag{4}$$

$$\mathrm{FS} = k\log_{10}(\min(V_{S30}, 1500)/800) \tag{5}$$

In the equations, M_w represents the seismic magnitude; R_{jb} represents the Joyner–Boore distance, defined as the shortest horizontal distance to the surface projection of the rupture plane (km); the greater the distance, the lower the median value; and V_{S30} represents the time-averaged shear-wave velocity in the upper 30 m (m/s); the smaller the value, the softer the site and the stronger the amplification effect.

Perform Kriging regression using the mean value of physical attenuation from ITA18 as a condition, and perform Kriging interpolation on the station residuals [18]:

$$\ln \mathrm{PGV}(\boldsymbol{x}) = \ln \mathrm{PGV}_{\mathrm{med}}(\boldsymbol{x}) + \hat{\varepsilon}(\boldsymbol{x}) \tag{6}$$

where $\ln \mathrm{PGV}_{\mathrm{med}}(\boldsymbol{x})$ is the median trend in physical attenuation, and $\hat{\varepsilon}(\boldsymbol{x})$ is the estimated residual. In the far field, the residuals decay to 0, and the prediction automatically degenerates into the distance attenuation described by Equation (1); in the near field, the measured corrections are retained, and only deviations outside the trend are corrected.

The spatial structure of the residual field is described by an exponential covariance model, whose range and nugget effect are obtained by fitting station residuals (Table 1). Conditional random simulations are performed around the conditional mean, and 1,000 spatially correlated ground motion scenarios are generated using the Cholesky decomposition of this covariance matrix [17]:

$$\ln \mathrm{PGV}^{(r)} = \boldsymbol{\mu}_{\mathrm{cond}} + \boldsymbol{L}\boldsymbol{z}^{(r)}, \boldsymbol{z}^{(r)} \sim \mathrm{N}(\boldsymbol{0}, \boldsymbol{I}) \tag{7}$$

where $\boldsymbol{\mu}_{\mathrm{cond}}$ is the conditional mean vector; $\boldsymbol{L}$ is the Cholesky factor of the conditional covariance matrix; and $\boldsymbol{z}^{(r)}$ is a standard normal random vector. These scenarios cause the PGV of each pipe segment to follow a log-normal distribution, with adjacent pipe segments tending to deviate from the median value simultaneously.

2.2 Pipe Segment Failure and Network Service Loss Metrics

The hazard field provides continuous intensity, while network consequence assessment requires discrete pipe segment states. This paper adopts the ALA empirical repair-rate relationship for strong ground motion, treating damage along a pipe segment as random independent events. The probability that pipe segment i experiences at least one damage instance under scenario r is given by [1, 11, 19-20]

$$P_{\mathrm{f}}^{(r,i)} = 1 - \exp\left(-K_1 k_i C_0 \mathrm{PGV}_{r,i} L_i\right) \tag{8}$$

where $\mathrm{PGV}_{r,i}$ is the peak ground velocity (cm/s) at the midpoint of the pipe segment; L_i is the length of the pipe segment (km); the higher the intensity and the longer the segment, the greater the probability of failure; $C_0 = 0.002416$ is a proportional constant; K_1 is an overall correction factor; and k_i is the segment-specific vulnerability coefficient, which increases as the rock type becomes softer or the pipe diameter decreases. The condition of each pipe segment is determined by sampling according to Equation (8) for each scenario; damaged pipe segments are treated as unavailable in network calculations. Failures in individual pipe segments are driven by the spatially correlated PGV field within the same scenario, while the correlation between failures across pipe segments is accounted for by the spatial correlation of the scenario field, rather than treating the conditions of individual pipe segments as independent across scenarios [21-22].

Pipe segment states describe only individual damage; the overall service loss of the pipeline network must be calculated separately. This paper uses the proportion of demand nodes still connected to gas supply inlets as a metric and quantifies the extent of damage by counting the number of failed pipe segments [11, 23]. Let the set of failed pipe segments be A; the network after removing A is $G(A)$; and the set of nodes connected to any gas supply inlet is $C_{\mathrm{s}}(A)$. Then, the gas supply connectivity rate is

$$R(A) = \frac{1}{|N_{\mathrm{d}}|}|C_{\mathrm{s}}(A) \cap N_{\mathrm{d}}|, C_{\mathrm{s}}(A) = \bigcup_{s \in N_{\mathrm{s}}} \mathrm{comp}_{G(A)}(s) \tag{9}$$

The service loss rate is defined as its complement: $1 - R(A)$; when all pipeline segments fail, it is set to 1.

2.3 Pipe Segment Contribution Allocation and Risk-Weighted Scoring in Cooperative Games

Manpower for post-earthquake inspections is limited; therefore, the assessment must rank the importance of individual pipeline segments to determine priority. The importance of a pipeline segment is determined by two factors: its own probability of damage in the current earthquake and its position within the pipeline network topology. Ranking based solely on failure probability overlooks location information; ranking based solely on static topological indicators (such as centrality or betweenness) overlooks seismic motion information, as the ranking remains unchanged for the same topology across different earthquakes; and simulating the removal of individual pipeline segments one by one can only

reveal the consequences of a single failure, failing to account for the combined effects of multiple segments failing simultaneously—which is the norm in post-earthquake scenarios.

This paper introduces the Shapley value from cooperative games to allocate the service loss rate of the entire network to individual pipeline segments. The Shapley value distributes total value based on marginal contribution without presupposing a specific network model; it allows the service loss rate resulting from the removal of a set of pipeline segments to be directly treated as a value function [12-13]. In this study, the participants are 168 pipeline segments, and the allocation target is the service loss rate. Let the service loss rate after removing the set of failed pipeline segments A be denoted as $v(A) = 1 - R(A)$. Then, the Shapley structural contribution S_i of pipeline segment i is

$$S_i = \sum_{A \subseteq E \setminus \{i\}} \frac{|A|!(|E|-|A|-1)!}{|E|!} [v(A \cup \{i\}) - v(A)] \tag{10}$$

where E denotes the set of all pipeline segments; $v(A \cup \{i\}) - v(A)$ denotes the marginal contribution after adding pipeline segment i. A fully intact network satisfies $v(\emptyset) = 0$, and when all segments fail, $v(E) = 1$; therefore, the sum of the Shapley contributions S_i for all segments equals 1. This paper uses 2,000 random permutations to approximate the Shapley values and performs 2,000 permutation bootstrap resamples.S_i is determined solely by the pipeline network topology and the selection of supply and demand nodes, and does not include seismic motion information.

To comprehensively reflect structural importance and seismic hazard, the expected probability of failure (f_i) is introduced to construct a risk-weighted score (W_i):

$$f_i = \frac{1}{M} \sum_{r=1}^{M} P_{\mathrm{f}}^{(r,i)}, W_i = S_i \cdot f_i, M = 1000 \tag{11}$$

f_i is calculated as the analytical average of the conditional failure probabilities across 1,000 scenarios, rather than the sampled failure frequency, to eliminate the additional variability introduced by damage sampling.$W_i = S_i f_i$ requires that the two factors be separable: S_i must be determined solely by topology and exclude PGV in order to be multiplied by the hazard field; if the expected damage probability is incorporated into the allocation criterion, this decomposition no longer holds.

3 METHODOLOGY OF THIS PAPER

3.1 Study Area, Pipeline Network, and Strong-Motion Records

The study focuses on the natural gas transmission pipeline network in Italy and the Norcia earthquake that occurred on October 30, 2016, at 06:40 UTC (Figure 1). The pipeline network data was obtained from the Italian sub-region of SciGRID_gas and projected onto UTM 33N after two rounds of restoration: multi-segment lines were split into single-segment lines, and endpoints were merged with millimeter precision to avoid the creation of pseudo-nodes [24]. The result is a single, connected pipeline network consisting of 168 pipeline segments and 94 nodes, with a total length of 7,704.6 km and segment lengths ranging from 1.9 to 145.6 km. The gas supply entry points were identified as the two access points at Gela and Mazara del Vallo, each matched to the nearest network node, resulting in $N_{\mathrm{s}} = \{1,4\}$; the remaining 92 nodes are demand nodes N_{d}.These two points are taken from the “EntryPoints” layer of the dataset; the same dataset records the three northern cross-border entry points—Tarvisio, Gorizia, and Passo Gries—in the “BorderPoints” and “InterConnectionPoints” layers. In the pipeline network topology, these three correspond to nodes 90, 81, and 94, respectively. For the purposes of this paper, they are uniformly treated as demand nodes, i.e., it is assumed that post-earthquake gas supplies enter only through the two southern entry points. The implications of this assumption are quantified in Section 4.2. The pipeline network runs north-south along the Apennine Peninsula, spanning approximately 1,150 km, as shown in Figure 2.

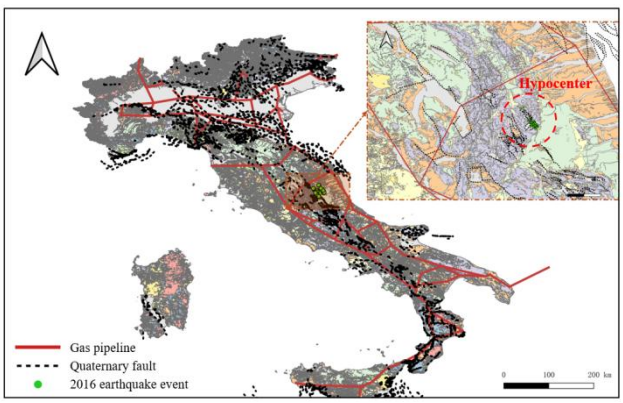


Figure 1 Study Area: Pipeline Network, Quaternary Faults, and the 2016 Norcia Earthquake[25]
Source: https://doi.pangaea.de/10.1594/PANGAEA.935673?format=html#download

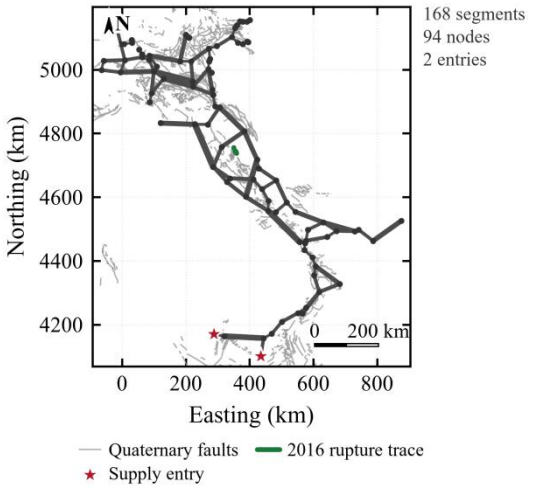


Figure 2 Pipeline Network Topology and Gas Supply Entry Points[25]
Source: https://doi.pangaea.de/10.1594/PANGAEA.935673?format=html#download

Pipeline segment attributes include site conditions, nominal diameter, and length. Length and nominal diameter are taken from the boundary table; site conditions are specified by lithological combinations, with the 19 lithological types across the entire network classified into three categories—hard rock, soft rock, and loose soft soil—based on their mechanical properties. Under the same seismic intensity, the repair rate per unit pipe length for loose soft soil sections is 2.3 to 2.8 times that of hard rock sections [19]. Pipeline segment length is included as a core variable in the exponential term of Equation (8); the longest single segment is 145.6 km, and the variation in geometric span across the entire network is far greater than the variation in site conditions along the route.Double counting of site effects in the relationship between hazard zones and vulnerability is avoided by uniformly assigning the V_{S30} value at the midpoint of each pipeline segment to 555 m/s, the median of measurements from 77 stations, without relying on lithological mapping.

Seismic source parameters and station records were both obtained from the ESM Strong Motion Database [26]: M_w 6.6, epicenter at 42.84°N, 13.12°E, depth 6.2 km, normal fault solution (strike 160°, dip 40°, rake −90°), consistent with the reference mechanism in ITA18; therefore, the mechanism correction term in Equation (2) is 0. The intensity metric used was RotD50 PGV. During screening, records were retained where both PGA and PGV were positive and where RotD50 PGA was higher at the same station, resulting in 175 stations. PGV ranged from 0.277 to 86.17 cm/s, with a median of 3.96 cm/s. A "measurements-first, fallback" strategy was adopted for station locations: for 77 stations with measured V_{S30} values, the measured values were used directly; for the remaining 98 stations, representative values were selected based on the EC8 site category from geological maps. Observation points are concentrated around the epicenter, while the pipeline network spans approximately 1,150 km, as shown in Figure 3.

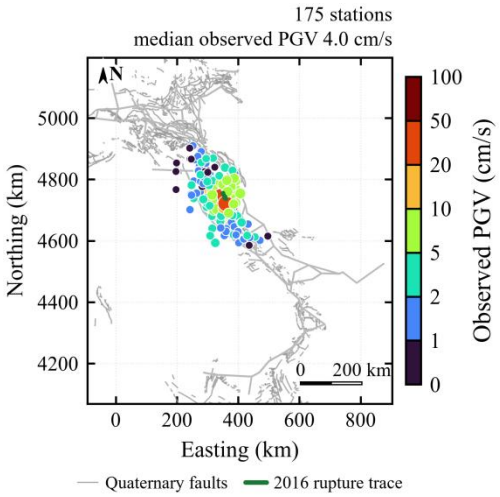


Figure 3 Spatial Distribution of Observed Station PGV[25]
Source: https://doi.pangaea.de/10.1594/PANGAEA.935673?format=html#download

R_{jb} was calculated based on the 2016 co-seismic surface rupture trace, which is the union of 17 segments of the M. Vettore fault system from the ITHACA database; the shortest distance from each point to the trace was calculated [27]. Since the trace represents the projection of surface rupture, while R_{jb} is defined as the shortest horizontal distance to the surface projection of the rupture plane, using the trace distance directly would result in a systematic overestimation.

Calibration was performed using the ESM data at R_{jb} $(n = 175)$, with a correlation coefficient of 0.993; the deviation is independent of distance and is attributed to geometric offset. Based on this, the overall offset is 11.0 km, and $R_{jb} = \max(d_{\text{trace}} - 11.0,\ 0.5)$ is adopted, with the lower limit chosen to prevent divergence of the logarithmic term. The median value for the R_{jb} of the pipeline segments is 353.7 km; among these, 3 segments are within 50 km, while 136 exceed 200 km. Due to the scarcity of near-field samples, the conclusions primarily apply to far-field pipeline segments; see Figure 4.

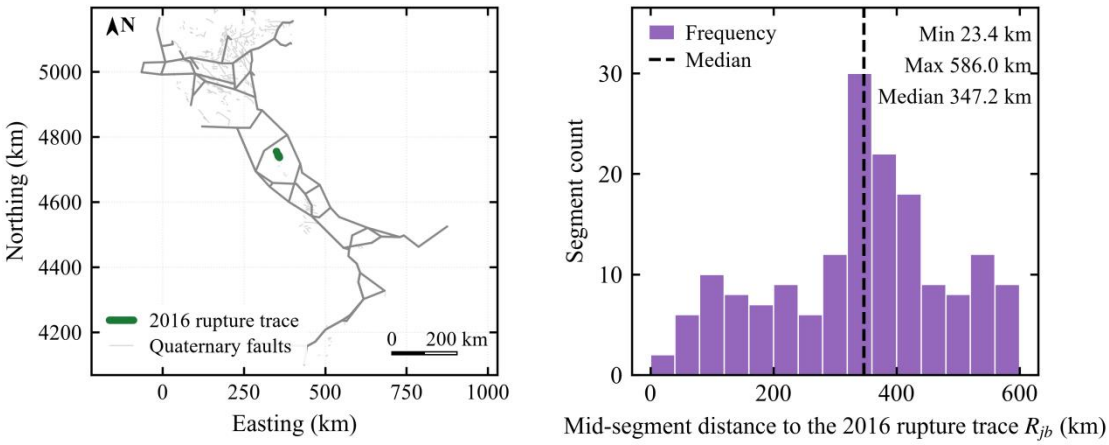


Figure 4 Definition of the "R_{jb}" and Trace-Offset Calibration. (a) What R_{jb} is measured to; (b) R_{jb} distribution[25]
Source: https://doi.pangaea.de/10.1594/PANGAEA.935673?format=html#download

3.2 Post-Earthquake Service Consequence Assessment Process

The process for assessing post-earthquake service consequences is shown in Figure 5. Spatially correlated seismic motion scenarios are constructed from station records, and the expected failure probability for each pipeline segment is determined through failure assessment; the service loss rate is calculated based on network connectivity following scenario-based failures, and the structural contribution of each individual pipeline segment is then allocated according to Shapley values; the structural contribution is multiplied by the expected failure probability to form a risk-weighted score, which is used to prioritize inspection sequences. The service loss rate quantifies the loss across the entire network, while the structural contribution and risk-weighted score characterize the distribution of losses among pipeline segments.

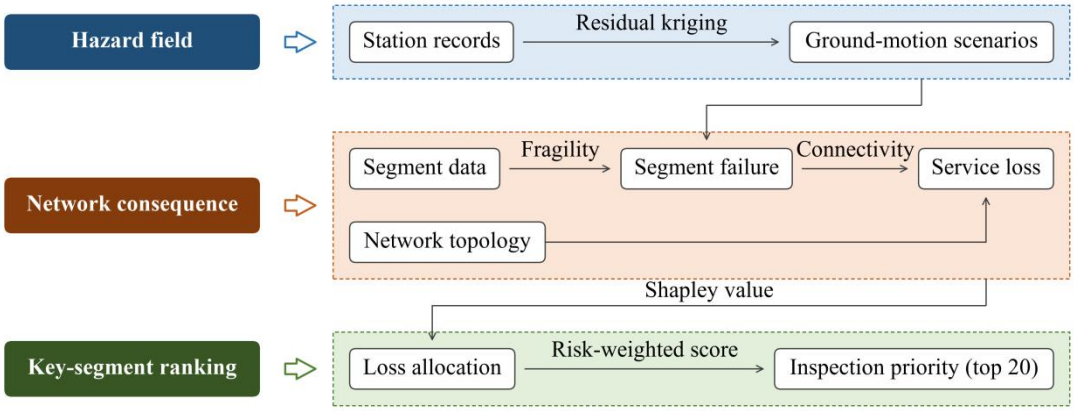


Figure 5 Post-Earthquake Service-Consequence Assessment Workflow

4 RESULTS

4.1 Validation of the Hazard Field

First, the "leave-one-out" method was used to compare the performance of three spatial interpolation models—inverse distance weighting (IDW), ordinary kriging (OK), and radial basis function (RBF)—across 175 monitoring stations, as shown in Figure 6. OK exhibited the highest accuracy in areas with dense station coverage, outperforming RBF and IDW; however, its effective range is limited by the range of the variogram: the PGV fitted from the stations yielded a variogram range of only 141.8 km, with most pipeline segments falling outside this range; the median variance of the midpoint

kriging was 1.997, and the predicted values collapsed to a single constant. Regression Kriging uses the mean value under physical attenuation as a condition and station residuals for correction.

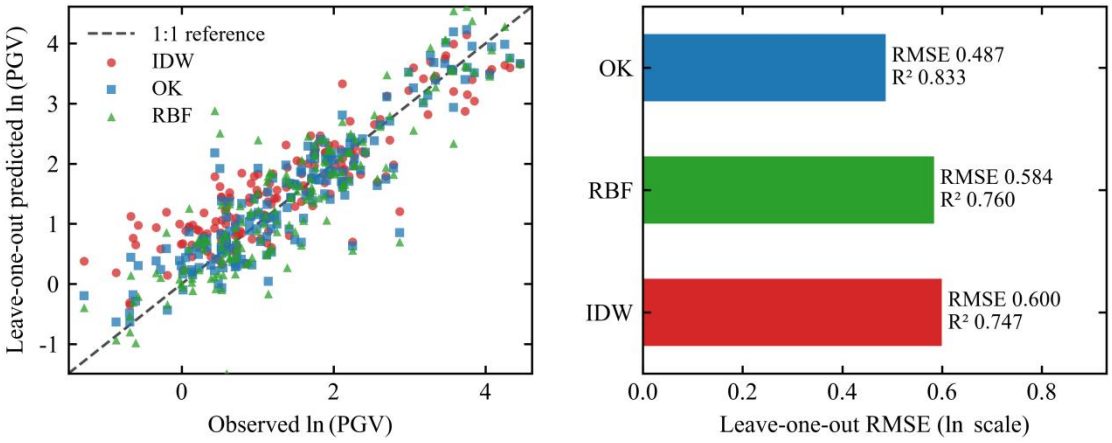


Figure 6 Leave-One-Out Comparison of Three Interpolation Models. (a) Observed vs. predicted; (b) Error comparison

Using ITHACA fracture trace lines as the distance reference, the PGV for 175 stations was predicted based on the Joyner–Boore distance used in ITA18. Site conditions were handled by prioritizing measured data and using proxy values when measurements were unavailable—referred to as the "site-priority strategy"—which constitutes the main result of this paper [10]; two control groups were also established: one using only measured stations (77 stations) and another using the entire bedrock, as shown in Table 1.

Table 1 Station-Level Validation of the ITA18 Trend and Residual Field Parameters under Three Station Site Strategies

Strategy	Number of Stations	Measured V_{S30}	Median Deviation Multiple	R^2	RMSE(ln)	Range (km)	Nugget variance
Site Selection (Main Results)	175	77	0.955	0.763	0.581	360.6	0.643
Measuring stations only	77	77	1.023	0.865	0.425	18.7	0.000
All bedrock	175	77	1.054	0.813	0.516	360.6	0.959

In terms of validation metrics, only the "measured stations" strategy performs better: median deviation of 2.3%, and a 0.102 higher value for the R^2. This strategy excludes 98 stations that have PGV measurements but lack V_{S30} data, resulting in an artificially high goodness-of-fit; its residual field range is only 18.7 km, which produces virtually no correction on a 1,150 km pipeline network. The deviations by distance are shown in Figure 7.

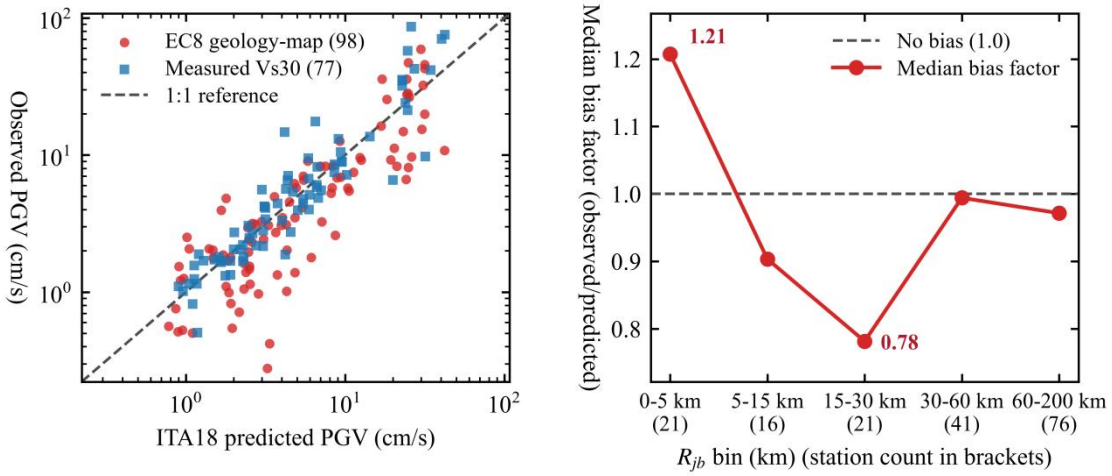


Figure 7 Station-Level Validation of ITA18. (a) Station-level observed vs. predicted; (b) Bias by distance

When binned by R_{jb}, the field-optimized estimates in the 15–30 km bin were underestimated by 22%; the median deviation multiple for the 10 observed stations in the same bin was 0.88, while that for the 11 proxy stations was 0.74. In all bins beyond 5 km, the proxy stations showed lower values ranging from 0.64 to 0.88, whereas the observed stations in the far field approached 1.00.

The standard deviation of residuals is 0.569 (ln), higher than the log standard deviation of 0.194 for the ITA18 event; the conditional random field generates fluctuations between scenarios based on the former, and the difference stems from the simplified treatment of source parameters and site conditions [10]. The leave-one-out error for Regression Kriging is 0.459, which is better than the 0.581 for the pure trend field.

A comparison of PGV at the midpoints of 168 pipe segments between OK interpolation (baseline field) and regression kriging (site-optimized) shows that beyond 200 km, the site-optimized method differs from the ITA18 pure trend by only 5%–7%, whereas the baseline field inflates this value to 4.8–8.7 times that of the pure trend. The baseline field degrades far from observation stations; 74% of the 168 pipe segments are more than 100 km from the nearest station, and within this range, the Kriging variance has reached its far-field asymptotic value, meaning the interpolation no longer provides observational information. A segment-by-segment comparison of the two fields is shown in Figure 8.

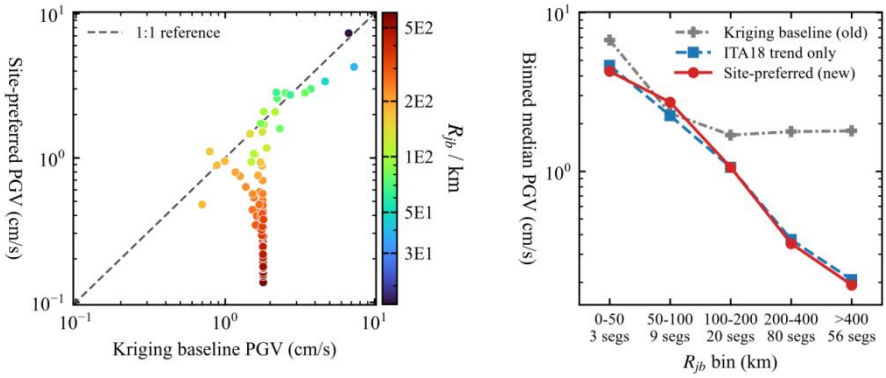


Figure 8 Segment-Wise Comparison of Previous and New PGV. (a) Segment-wise PGV: site-preferred vs. baseline; (b) Binned median PGV

4.2 Post-Earthquake Network Service Loss

The status of each segment was determined and network consequences were calculated for 1,000 spatially correlated ground motion scenarios; see Table 2.

Table 2 Network Service Consequences (Mean of 1,000 Scenarios)

Indicator	Baseline Field	Site-Optimized	Change
Average Number of Failed Pipeline Sections	40.07	12.08	−70%
Service Loss Rate	0.766	0.334	−56%
Gas Supply Connectivity Rate	0.234	0.666	+185%

The average number of failed pipe segments decreased from 40.1 to 12.1, and the service loss rate decreased from 0.766 to 0.334: the consequences for the baseline field were 2.3 times those of the site-optimized strategy; this difference stems from the degradation of the baseline field in the far field, rather than the site-optimized strategy being too conservative. The average service loss for the other two site selection strategies was 0.388 and 0.393, respectively, which were 16% and 18% higher than the main result; the site selection strategies did not alter the order of magnitude. The service loss distribution for the main result was bimodal: 455 scenarios fell below 0.27, 537 fell above 0.51, and only 8 scenarios fell within this range, as shown in Figure 9.

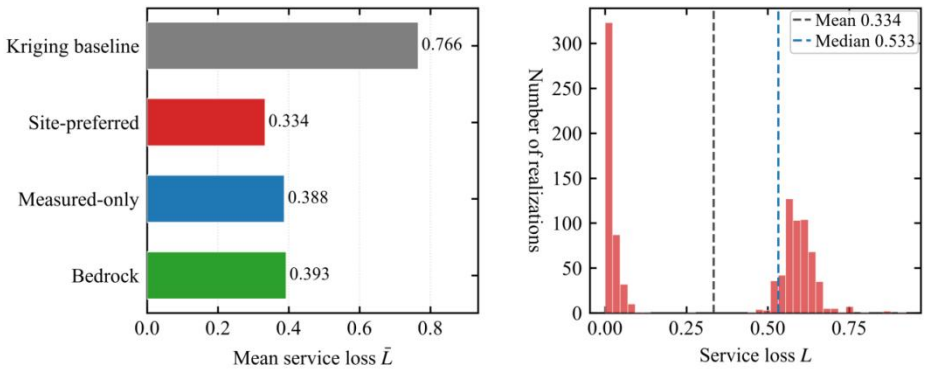


Figure 9 Network Service Consequences. (a) Mean loss by field construction; (b) Loss over 1000 realizations

The bimodal distribution stems from the network structure. The 455 scenarios in the low-loss peak involved an average of 10.9 failed pipe segments, with a mean loss of 0.021; the 537 scenarios in the high-loss peak involved an average of

13.0 failed pipe segments, with a mean loss of 0.597. Although the difference in the number of failed segments between the two peaks is only 2.1, the loss differs by a factor of 29. The key distinction lies in whether the failed segments fall within or outside the channels leading to the north: In the high-loss peak, 500 scenarios (93%) resulted in a complete loss of connectivity for nodes 47–94. These 48 demand nodes account for 52% of all demand nodes, and only one channel connects them to the gas supply inlet; Failures in pipeline segments outside the corridor result in only localized losses.
The selection of entry points, on par with site selection strategies, alters the magnitude of the consequences. When the three northern cross-border access points (nodes 90, 81, and 94) were also counted as gas supply entry points and the calculations were redone, the service loss rate dropped from 0.334 to 0.032, the gas supply connectivity rate rose from 0.666 to 0.968, and the number of scenarios with losses exceeding 0.51 decreased from 537 to 0, thereby eliminating the double peak, and the maximum scenario loss decreased from 0.924 to 0.419; when the three LNG receiving terminals at Panigaglia, Porto Levante, and Toscana (nodes 48, 56, and 45) were included, the service loss rate further decreased to 0.023. The average number of failed pipeline segments across the three inlet scenarios was 12.08: pipeline segment failure is determined solely by seismic motion, and the inlet scenarios only affect which demand nodes can still be reached from the gas source after the failure.

4.3 Identification of Critical Pipeline Segments and Inspection Prioritization

The risk-weighted scores are $W_i = S_i f_i$: S_i is determined solely by the pipeline network topology and the selection of gas supply inlets and demand nodes, while f_i represents the expected failure probability of a pipeline segment across 1,000 scenarios. The top 20 entries for W_i under the site optimization strategy are shown in Table 3.

Table 3 Top 20 Segments by Risk-Weighted Shapley Value

Rank	Pipe Segment ID	S_i	f_i	W_i
1	340	0.02415	0.3473	0.008387
2	323	0.08788	0.0892	0.007842
3	329	0.00960	0.6325	0.006074
4	346	0.10666	0.0411	0.004385
5	311	0.00664	0.5643	0.003748
6	68	0.01347	0.2052	0.002764
7	330	0.00343	0.7807	0.002677
8	296	0.00563	0.4153	0.002339
9	69	0.00719	0.3184	0.002290
10	269	0.01097	0.1746	0.001915
11	118	0.00419	0.4369	0.001831
12	129	0.00487	0.3606	0.001756
13	339	0.01103	0.1585	0.001749
14	270	0.00990	0.1746	0.001729
15	128	0.00470	0.3368	0.001582
16	64	0.00628	0.2434	0.001528
17	412	0.00322	0.4613	0.001487
18	59	0.01055	0.1365	0.001440
19	413	0.00264	0.4613	0.001219
20	328	0.00690	0.1748	0.001206

The score difference between the top two segments is only 6.5%, and the difference (5.5×10^{-4}) is less than the paired standard error (9.0×10^{-4}); in 2,000 bootstrap simulations, segment 340 ranked first in 72% of the simulations, while segment 323 ranked first in 26% of the simulations. Therefore, these two segments are listed only as the two with the highest scores, in no particular order, as shown in Figure 10.

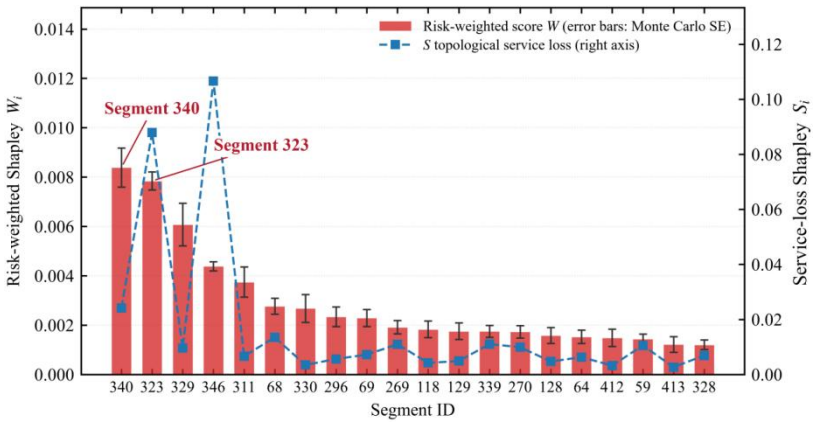


Figure 10 Top 20 Segments by Risk-Weighted Shapley Value

The two factors are nearly independent: the rank correlation between S_i and f_i is only 0.176, with a linear correlation of 0.035; their dynamic ranges are 1,963-fold and 301-fold, respectively. The two highest-scoring segments compensate for each other: the S_i for segment 323 is 3.64 times that of segment 340, while the f_i for segment 340 is 3.89 times that of segment 323. Pipe segment 346's "S_i " score was the highest in the entire network, while its "f_i " score ranked only 61st, dropping it to 4th place; among the top 5 segments by structural contribution, 3 (257, 178, 177) did not make the top 20. Only 4 pipeline segments overlap between the top 20 ranked by "S_i " and those ranked by "W_i "; W the top 20 segments' S rankings span from 1st to 83rd place, and prioritizing inspections based solely on topological contribution would omit 16 critical pipeline segments.

The top 20 are determined by a combination of location and hazard level. Location provides the necessary condition: of the 48 demand nodes at nodes 47–94, only one corridor connects them to the gas supply inlet; if this corridor is interrupted, they all lose gas supply, accounting for 52% of the network's demand nodes. The network's only two single-segment critical pipeline segments, 346 and 323, are both located on this corridor; Removing either of these two segments individually results in a service loss exceeding 0.51, whereas removing any other pipeline segment in the network individually results in a service loss of no more than 0.033. Risk screening criteria: The southern trunk line near the gas inlet also cuts off large downstream areas, with a "S_i " that is not low, while the "f_i " ranges from only 0.01 to 0.05; pipeline segments within the corridor also require sufficiently strong seismic motion. Eighteen of the 20 segments fall within the section spanning nodes 29–46, while the remaining two—segments 323 and 59—are located within the northern node cluster.

The structural contribution S_i is defined jointly by the pipeline network topology, gas supply entry points, and demand nodes. Table 3 shows the allocation results based on the two access points at Gela and Mazara del Vallo; the listed pipeline segments are those prioritized for post-earthquake inspection, and their spatial distribution is shown in Figure 11. When recalculated based on a scenario including the three northern cross-border access points, 17 of the top 20 segments overlap with those in Table 3; segment 346 drops out of the top 20, and the top-ranked segment changes from 340 to 329.

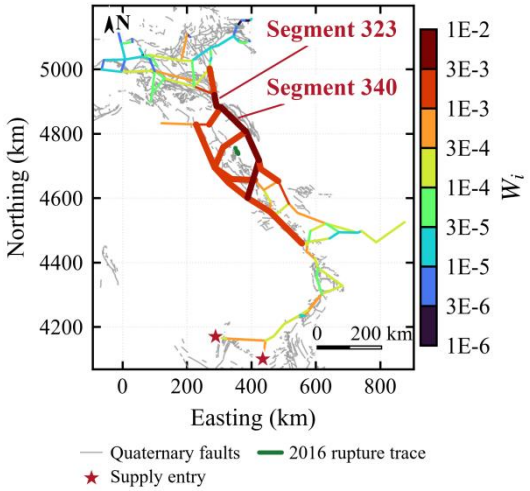


Figure 11 Spatial Distribution of Key Segments[25]
Source: https://doi.pangaea.de/10.1594/PANGAEA.935673?format=html#download

5 DISCUSSION

Post-earthquake service losses in pipeline networks are jointly determined by the spatial correlation structure of the seismic motion field, the location of failed pipeline segments within the network, and the network's connectivity to demand nodes [21-22, 28]: Seismic motion intensity determines which pipeline segments fail, while the location of these failed segments determines whether these failures result in service interruptions [23, 29]. For hazard fields, previous studies have either modeled the residuals of attenuation relationships as two-dimensional random fields or directly used covariance models to simulate spatially varying ground motion, all of which treat spatial correlation as central to scenario generation; this paper is consistent with this approach [21, 30]; The difference lies in the fact that purely statistical covariance models do not incorporate physical attenuation, and the far field can only be inferred through model assumptions; in contrast, this paper uses physical attenuation relationships to derive far-field trends, while the covariance model is used solely to interpolate station residuals. This distinction is decisive when stations are sparsely distributed: 74% of pipeline segments are more than 100 km from the nearest station. Pure interpolation predictions collapse to a single constant over these segments, inflating the PGV beyond 200 km to 4.8–8.7 times that of the pure trend, causing the service loss rate to rise from 0.334 to 0.766; Regression Kriging exhibited deviations of only 5%–7% over the same interval, with a "leave-one-out" error of 0.459, outperforming the 0.581 error of the pure trend field. Furthermore, regarding network consequences, existing studies have measured post-earthquake functional losses using metrics such as global efficiency and service loss rate, and have incorporated the spatial variability of the ground motion field into connectivity reliability assessments [23, 28-29]. This study further finds that service loss does not vary monotonically

with the number of failed segments: the average number of failed pipe segments at the two peaks of the service loss distribution differs by only 2.1 segments, yet the loss differs by a factor of 29. This discrepancy stems from whether the failed pipe segments fall on or outside the sole pathway to a demand cluster; therefore, the measurement of network consequences must retain the spatial dimension; Allocating service loss to individual pipe segments based on marginal contribution using Shapley values is a step toward mapping system-level metrics to specific segments within the same scenario. The top 20 segments ranked by risk-weighted scores and those ranked by structural contribution overlap by only 4 segments, indicating that both location and hazard must be considered in the ranking [12-13, 31-32].

This paper still has two shortcomings. On the one hand, the hazard field simplifies the earthquake source to a single rupture surface and a pure fault, with distance represented solely by an 11.0 km overall offset along trace lines; permanent ground displacement and fault displacement are not accounted for. The site parameter V_{S30} is uniformly set at 555 m/s to avoid double-counting site effects with lithological coefficients; as a result, local site amplification may be overlooked; The standard deviation of residuals, 0.569(ln), does not distinguish between observational noise and modeling errors; furthermore, the dataset consists of only one event and one magnitude, with a low proportion of near-field pipeline segments, resulting in limited extrapolation capability. On the other hand, the repair rate relationship and segment-by-segment vulnerability coefficients were derived from lithological-diameter mappings within the water supply system and the project, respectively, and were not calibrated using pipeline seismic damage data; Damaged pipeline segments were treated as unusable, and service loss was calculated only as the initial post-earthquake value, without accounting for the repair sequence; for gas supply entry points, only the two southern locations in the "EntryPoints" layer of the dataset were included, while cross-border entry points in the northern part of the pipeline network were treated as demand nodes. Both the service loss rate and the ranking of critical pipeline segments were limited to this entry point scenario. Future work will incorporate events with multiple seismic magnitudes and various source mechanisms, calibrate vulnerability coefficients using measured site parameters and pipeline seismic damage data, and integrate the repair sequence into the recovery process.

6 CONCLUSIONS

(1) Regression kriging, which uses the physical attenuation of ITA18 as the mean and station residuals as Kriging corrections, provides a hazard field that incorporates both distance attenuation and local corrections under sparse station conditions. In this case study, 81% of the pipeline segments had $R_{jb} > 200$ km, while 74% were more than 100 km from the nearest station. The OK method predicted a constant PGV value across these segments, elevating the PGV beyond 200 km to 4.8–8.7 times that of the pure ITA18 trend, causing the service loss rate to increase from 0.334 to 0.766; The leave-one-out cross-validation error for regression kriging was 0.459, which is better than the 0.581 for the pure trend field.

(2) Under 1,000 spatially correlated seismic motion scenarios, the average number of failed pipeline segments in this network was 12.1, with a service loss rate of 0.334 and a gas supply connectivity rate of 0.666; When switching to site strategies using only measured stations and all-bedrock sites, the service loss rates were 0.388 and 0.393, respectively—16% and 18% higher than the main results, though the order of magnitude remained unchanged. By allocating the service loss rate to individual pipeline segments based on Shapley values to determine structural contributions, and then multiplying these by the expected failure probability, the priority order for post-earthquake inspections was established: The dynamic range of structural contributions across segments was 1,963-fold. Among the top 20 segments by score, 18 were located on routes serving demand nodes in the northern part of the service area; these included both Segment 346, which had the highest structural contribution, and Segment 330, which had the highest probability of damage in this earthquake.

(3) This method is suitable for pipeline networks where location-sensitive service loss is the allocation criterion; the more dispersed the distribution of demand nodes and the greater the geographical variation, the more applicable the method becomes. Due to the limitations of a single event and a single seismic magnitude, only 12 of the 168 pipeline segments in this study had $R_{jb} < 100$ km, resulting in limited extrapolation capability for near-field conclusions; the vulnerability coefficients for each segment were derived from an internal project lithology-to-pipe-diameter mapping and were not calibrated against publicly available vulnerability models; the analysis scope was limited to initial service loss following the earthquake, without accounting for the impact of repair sequencing on recovery trajectories [33]; for gas supply entry points, only the two southern locations in the EntryPoints layer of the dataset were considered, while the three cross-border access points in the northern part of the pipeline network were treated as demand nodes; both the service loss rate and inspection sequencing were restricted to this entry scenario. Future research could incorporate finite fault models and event records with multiple magnitudes and different source mechanisms, perform calibration using measured site parameters and pipeline seismic damage data, and integrate repair sequencing into the recovery process.

COMPETING INTERESTS

The authors have no relevant financial or non-financial interests to disclose.

FUNDING

This work was supported by the Scientific Research Fund of Guangdong University of Petrochemical Technology and the Special Fund for the 2025 Guangdong Provincial College Student Innovation Training Program (Project "Oil and Gas Pipeline Network Earthquake Monitoring and Early Warning Platform", Grant No. 25B096).

REFERENCES

[1] Esposito S, Iervolino I, d'Onofrio A, et al. Simulation-Based Seismic Risk Assessment of Gas Distribution Networks. Computer-Aided Civil and Infrastructure Engineering, 2015, 30: 508–523.
[2] Lanzano G, Salzano E, de Magistris F S, et al. Seismic vulnerability of natural gas pipelines. Reliability Engineering & System Safety, 2013, 117: 73–80.
[3] O'Rourke T D, Palmer M C. Earthquake Performance of Gas Transmission Pipelines. Earthquake Spectra, 1996, 12: 493–527.
[4] Shimizu Y, Yamazaki F, Isoyama R, et al. Development of Realtime Disaster Mitigation System For Urban Gas Supply Network. Proceedings of the 13th World Conference on Earthquake Engineering (13th WCEE), Vancouver, BC, Canada, 2004.
[5] Kwong N S, Jaiswal K S, Baker J W, et al. Earthquake Risk of Gas Pipelines in the Conterminous United States and Its Sources of Uncertainty. ASCE-ASME Journal of Risk and Uncertainty in Engineering Systems, Part A: Civil Engineering, 2022, 8: 04021081.
[6] Toprak S, Taskin F. Estimation of Earthquake Damage to Buried Pipelines Caused by Ground Shaking. Nat Hazards, 2007, 40: 1–24.
[7] Esposito S, Iervolino I. PGA and PGV Spatial Correlation Models Based on European Multievent Datasets. Bulletin of the Seismological Society of America, 2011, 101: 2532–2541.
[8] Worden C B, Thompson E M, Baker J W, et al. Spatial and Spectral Interpolation of Ground-Motion Intensity Measure Observations. Bulletin of the Seismological Society of America, 2018, 108: 866–875.
[9] Buratti N, Simoni E, Mazzotti C. Post-earthquake estimates of different ground motion intensity measures for the 2012 Emilia earthquake. Earthquake Engineering & Structural Dynamics, 2023, 52: 183–203.
[10] Lanzano G, Luzi L, Pacor F, et al. A Revised Ground-Motion Prediction Model for Shallow Crustal Earthquakes in Italy. Bulletin of the Seismological Society of America, 2019, 109: 525–540.
[11] Adachi T, Ellingwood B R. Serviceability Assessment of a Municipal Water System Under Spatially Correlated Seismic Intensities. Computer-Aided Civil and Infrastructure Engineering, 2009, 24: 237–248.
[12] Bachrach Y, Porat E, Rosenschein J S. Sharing Rewards in Cooperative Connectivity Games. Journal of Artificial Intelligence Research, 2013, 47: 281–311.
[13] Michalak T P, Aadithya K V, Szczepanski P L, et al. Efficient Computation of the Shapley Value for Game-Theoretic Network Centrality. Journal of Artificial Intelligence Research, 2013, 46: 607–650.
[14] Hengl T, Heuvelink G B M, Rossiter D G. About regression-kriging: From equations to case studies. Computers & Geosciences, 2007, 33: 1301–1315.
[15] Krige D G. A Statistical Approaches to Some Basic Mine Valuation Problems on the Witwatersrand. Journal of the Chemical, Metallurgical and Mining Society of South Africa, 1951, 52: 119-139.
[16] Georges Matheron. Principles of geostatistics. Economic Geology, 1963, 58(8): 1246-1266. DOI: 10.2113/gsecongeo.58.8.1246.
[17] Journel A G, Huijbregts Ch J. Mining Geostatistics. London: Academic Press. 1978.
[18] Odeh I O A, McBratney A B, Chittleborough D J. Further results on prediction of soil properties from terrain attributes: heterotopic cokriging and regression-kriging. Geoderma, 1995, 67: 215–226.
[19] American Lifelines Alliance. Seismic fragility formulations for water systems, Part 1: Guideline. American Lifelines Alliance, 2001.
[20] O'Rourke M, Ayala G. Pipeline Damage Due to Wave Propagation. Journal of Geotechnical Engineering, 1993, 119: 1490–1498.
[21] Wang M, Takada T. Macrospatial Correlation Model of Seismic Ground Motions. Earthquake Spectra, 2005, 21: 1137–1156.
[22] Zerva A, Zervas V. Spatial variation of seismic ground motions: An overview. Appl. Mech. Rev, 2002, 55: 271–297.
[23] Chang S E, Svekla W D, Shinozuka M. Linking Infrastructure and Urban Economy: Simulation of Water-Disruption Impacts in Earthquakes. Environ Plann B Plann Des, 2002, 29: 281–301.
[24] Pluta A, Medjroubi W, Diettrich J C, et al. SciGRID_gas - Data Model of the European Gas Transport Network. In: 2022 Open Source Modelling and Simulation of Energy Systems (OSMSES), 2022: 1–7.
[25] Bucci Francesco, Santangelo Michele, Fongo Lorenzo, et al. A new digital lithological Map of Italy at 1: 100.000 scale. PANGAEA, 2021. DOI: 10.1594/PANGAEA.935673.
[26] Luzi L, Puglia R, Russo E, et al. The Engineering Strong-Motion Database: A Platform to Access Pan-European Accelerometric Data. Seismological Research Letters, 2016, 87: 987–997.
[27] ITHACA Working Group. ITHACA (ITaly HAzard from CApable faulting), A database of active capable faults of the Italian territory (Version December 2019). ISPRA Geological Survey of Italy, 2019. http://sgi2.isprambiente.it/ithacaweb/Mappatura.aspx.

[28] Chen X, Miao H. Connectivity reliability analysis of urban power-gas systems considering spatial variability of ground motions. In: Zhao Y-G, Xu C, Chen F, et al. (Eds.), Proceeding of the 9th International Symposium on Lifeline and Infrastructure Earthquake Engineering. Springer Nature, Singapore, 2025: 493–501.
[29] Latora V, Marchiori M. Efficient Behavior of Small-World Networks. Phys. Rev. Lett., 2001, 87: 198701.
[30] Liao S, Zerva A. Physically compliant, conditionally simulated spatially variable seismic ground motions for performance-based design. Earthquake Engineering & Structural Dynamics, 2006, 35: 891–919.
[31] Narayanam R, Narahari Y. A Shapley Value-Based Approach to Discover Influential Nodes in Social Networks. IEEE Transactions on Automation Science and Engineering, 2011, 8: 130–147.
[32] Wang W, Cui G. A Shapley-value cooperative game-based risk decision model for natural gas pipeline vulnerability. Reliability Engineering & System Safety, 2026, 275: 112886.
[33] Ouyang M, Dueñas-Osorio L. Time-dependent resilience assessment and improvement of urban infrastructure systems. Chaos, 2012, 22: 033122.